

Inverse design of lightweight broadband reflector for efficient lightsail propulsion

Weiliang Jin,¹ Wei Li,¹ Meir Orenstein,² and Shanhui Fan¹

¹*Department of Electrical Engineering, Ginzton Laboratory, Stanford University, Stanford, California 94305, USA*

²*Department of Electrical Engineering, Technion-Israel Institute of Technology, 32000 Haifa, Israel*

Light can exert forces on objects, promising to propel a meter-scale lightsail to near the speed of light. The key to address many challenges in such an ambition hinges on the nanostructuring of lightsails to tailor their optical scattering properties. In this letter, we present a first exhaustive study of photonic design of lightsails by applying large-scale optimization techniques to a generic geometry based on stacked photonic crystal layers. The optimization is performed by rigorous coupled-wave analysis amended with automatic differentiation methods for adjoint-variable gradient evaluations. Employing these methods the propulsion efficiency of a lightsail that involves a tradeoff between high broadband reflectivity and mass reduction is optimized. Surprisingly, regardless of the material choice, the optimal structures turn out to be simply one-dimensional subwavelength gratings, exhibiting nearly 50% improvement in acceleration distance performance compared to prior studies. Our framework can be extended to address other lightsail challenges such as thermal management and propulsion stability, and applications in integrated photonics such as compact mirrors.

Light can exchange momentum with objects [1], leading to many vital breakthroughs in the field of nanotechnology such as optical tweezers for precise manipulation of nanoscale particles [2, 3]. Optical force can also play a crucial role in much larger lengthscale applications such as space travel, including the recent launch of solar sail driven by sun light [4]. Another and even more ambitious project is the Starshot Breakthrough Initiative that aims to accelerate a meter-size spacecraft to 20% of the speed of light, so that it can reach a nearby galaxy Proxima Centauri in 20 years [5, 6]. By far, the most plausible propulsion mechanism is based on optical force [7], or radiation pressure from GW/m² level lasers [8].

While such a project requires multidisciplinary efforts [6] such as materials science [9], mechanical engineering, astrophysics [10], and telecommunications [11], many key challenges can be alleviated via probing the boundary of photonic design, including efficient propulsion [8], heat management [12], laser beam focusing [13], and self-stabilization [14–17]. They all contain many tradeoffs that were so far optimized by tuning few geometric parameters of simple photonic structures, leaving possibly much room for improvement by systematically studying more complicated structures. An important tool for accomplishing this task is inverse design method capable of exploring millions of design variables that have been introduced into photonics in the last decade [18, 19], proving to be powerful in discovering structures whose performances hit theoretical bounds [20], or in suggesting the existence of tighter fundamental limits, e.g. recently improved bounds on optical absorption and scattering cross sections [21], optical force [22], near-field [23, 24] and far-field thermal radiation [25].

In this letter, as an initial step towards systemically pushing forwards photonics-related performances of lightsails, we apply large-scale optimization methods to identify lightsail geometric design criteria for optimal propulsion efficiency, crucial to lowering both laser power and phase array size [12]. More specifically, we seek to minimize a figure-of-merit (FOM) described by Eq. 1, known as acceleration distance that involves a tradeoff between broadband reflectivity and

lightsail mass. Previous optimizations were based on simple photonic crystal (PhC) slabs [8, 12], in contrast, here we explore a generic class of geometries, stacked PhC layers whose dielectric spatial profiles can be arbitrarily set within the unit cell. Gradient-based optimization methods are applied to simultaneously optimize over dielectric distributions, periodicity of PhC, and thickness of each layer, whose gradients are conveniently evaluated with automatic differentiation methods [26]. Different constituent materials of lightsails and payload mass are studied. Surprisingly, we demonstrate that for both high-index material such as silicon, and lower-index material such as silicon nitride, the optimal structure converges to a one-dimensional (1D) subwavelength grating, a robust solution against a wide range of payload mass. The FOM of this optimal structure exhibits a nearly 50% improvement against that of previously explored structures. The enhancement is attributed to the destructive interference of two guided modes that can be supported in such a grating of small material volume filling ratio and at a subwavelength thickness. The optimal solutions can converge to more complicated two-dimensional (2D) PhC structures when more emphasis is imposed on maximizing reflectivity, e.g. when the payload mass is large. Finally, we conclude that in general with optimizations, high-index material yields better performance.

In a general context, a broadband mirror is traditionally realized with a metallic reflector, which nevertheless possesses high material absorption loss, incompatible with the thermal management requirement of the Starshot projects [8]. Recent advances in nanotechnologies have led to the development of low-loss all-dielectric mirrors such as the distributed Bragg reflector [27], and several more compact schemes. One representative class of structures is derived from metamaterial principles by exploiting the single-negative response, commonly implemented with a single layer of microspheres, cubes [28–30], or shapes discovered with machine learning methods [31]. Another direction is based on guided-wave analysis that employs the double-mode destructive interference effect, realized with a subwavelength 1D grating of high-index contrast dielectrics [32, 33]. The mechanism of the two approaches can

be unified [34]. However, a comprehensive study on the mirror design principle for minimal mass is missing, a principle relevant in many integrated photonic applications, and in efficient propulsion of lightsails.

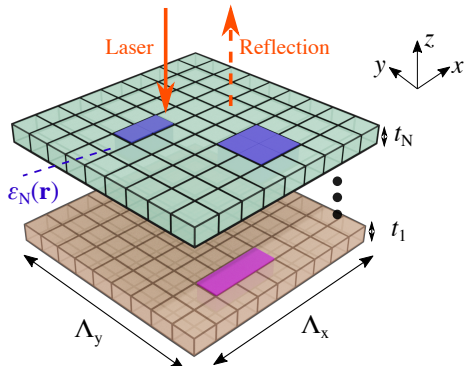


Figure 1: Schematic of a lightsail propelled by laser beams. The lightsail consists of stacked photonic crystal layers of period $\Lambda_{x(y)}$. The design space includes the period $\Lambda_{x(y)}$, the in-plane dielectric index value $\varepsilon_i(\mathbf{r})$ at each grid point, and the thickness t_i of the i -th layer. Here different colors represent different materials.

As shown in Fig. 1, we envision a spacecraft consisting of a payload (not shown) and a lightsail, where the latter is structured to enhance the optical force along the normal ($-z$) direction exerted on the sail by an incident high-power laser beam. From momentum conservation, the optical force increases with lightsail’s reflectivity [12, 35]. A practical FOM characterizing the propulsion efficiency is the distance D for the spacecraft to be accelerated to a target velocity, which takes into account the trade-off between optical force and kinetic quantities such as mass, which is captured by the following equation [7, 8],

$$D = \frac{c^3}{2I}(\rho_l + \rho_s) \int_0^{\beta_f} d\beta \frac{h(\beta)}{R[\lambda(\beta)]} \quad (1)$$

where $\rho_{s(l)}$ is the area density mass of the lightsail (payload), I the laser intensity, c the speed of light, and $h(\beta) = \beta/(1-\beta)^2 \sqrt{1-\beta^2}$ encodes relativistic factors depending on velocity fraction $\beta = v/c$. The integration is performed from stationary motion to a target velocity $c\beta_f$, and during this time interval the laser wavelength λ in the lightsail frame is Doppler redshifted from λ_0 to $\lambda(\beta) = \lambda_0 \sqrt{(1+\beta)/(1-\beta)}$. A representative value as in the Starshot project is $\lambda(\beta_f) \approx 1.22\lambda_0$, revealing that the reflectivity R of the lightsail needs to be enhanced over a large bandwidth. Minimization of D has a direct impact on reducing both the size of the laser phase array that needs to account for diffraction [12], as well as the total power consumption.

Optimization. To minimize D , we seek to structure the lightsail with wavelength or subwavelength features to tailor its optical scattering properties. Since the lightsail should involve two vastly different geometric scales, a macroscopic area $\sim 10 \text{ m}^2$ and nanoscale thickness on the order of 10^2 nm ,

the suitable generic class of geometries is stacked PhC slabs. As shown in Fig. 1, each layer i with thickness t_i is uniform along z -direction, and periodically structured in the xy -plane. Such a platform contains a rich library of geometries, including the aforementioned dielectric broadband mirrors, and previously explored lightsail structures such as uniform slabs, multilayer stacks, and PhC pillars or holes [8, 12]. Inverse design of more complicated geometries such as aperiodic structures including Moiré lattices and photonic quasicrystals for inherent broadband responses [36], and curved surfaces for mechanical stability [16], will be considered in a future work.

In order to probe the limit of D via photonic designs, we apply the “topology” optimization approach [18] that enables us to explore the largest possible design space. More specifically, we discretize the unit cell of the i -th layer into $M_i \times M_i$ grids, and allow to choose between materials at each grid point independently. This contributes to at least $\sum_{i=1}^N M_i^2$ design variables, each of which can take n discrete values, where N is the total number of layers, and n the number of candidate materials. We also treat the periodicity and the thickness of each layer as additional independent variables. The key to the tractability of such large-scale optimizations is the use of gradient-based optimization algorithms, such as the method of moving asymptotes [37]. To make use of these approaches, the index of refraction at each grid can initially vary continuously between various types of materials, and subsequently be binarized with filter and regularization methods [38]. However, such local optimization algorithms are known to be ill-behaved over high-index dielectric structures [39], due to the presence of many narrow-band resonances such as bound states in the continuum [40]. To better approach globally optimal solutions, we employ a relaxation method that broadens any high-Q response by adding fictitious material absorption loss to the entire system, and eventually turning it off [39]. By employing this approach, our optimization results are highly insensitive to initial parameters, a hint for possibly globally optimal results.

The primary complexity of inverse design problems lies in the derivation of the adjoint-variable problem for efficient gradient evaluation [18]. While our FOM in Eq. 1 is simple, future work in optimizing other aspects of lightsails may lead to convoluted FOMs that makes the derivation of gradient information mind-twisting. Thankfully, recent advancement in machine learning community has led to the development of various convenient packages for automatic differentiation, the application of adjoint-variable methods to arbitrary computational graphs [26]. With those tools, we only need to implement forward problems, while the backward gradient evaluations will be generated automatically. For efficient optimization of Eq. 1 over arbitrarily structured PhC layers, we have implemented a package [41] that extends rigorous coupled-wave analysis (RCWA) [42] with the automatic differentiation software Autograd [43].

Results. We apply the optimization formulation to identify the optimal structuring criteria that minimize D . A glimpse on Eq. 1 indicates that design criteria depend on the refrac-

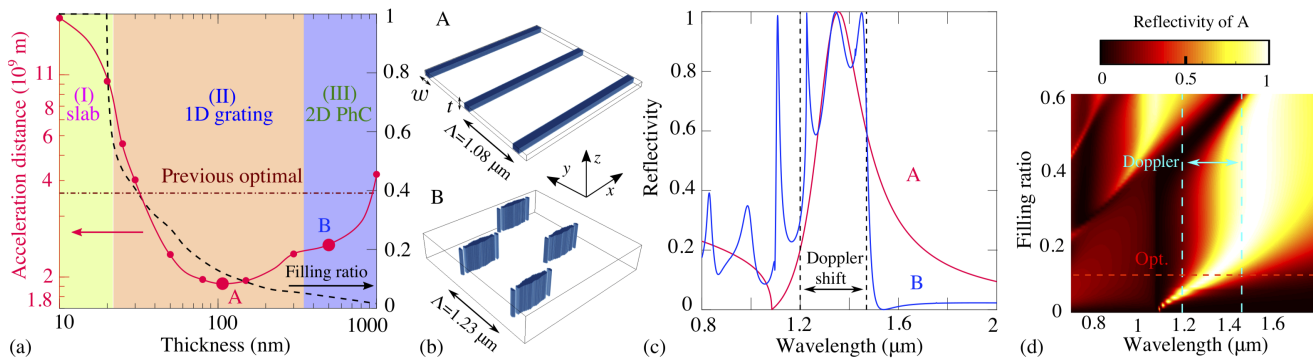


Figure 2: Inverse design of lightsail made of crystalline silicon. (a) acceleration distance (left axis) and filling ratio (right axis) of the structures optimized at each thickness, illustrate the transition of optimal geometry from uniform slabs (green), one-dimensional gratings (orange), to two-dimensional PhCs (purple). Red dash-dotted line denotes the previous optimal design [8]. Two representative structures at points *A* and *B* are illustrated in (b), and their calculated reflection spectrum is shown in (c). The *x*-polarized laser beam is propagating along $-z$ direction. (d) reflectivity of the optimal grating structure *A* as a function of wavelength and width w , or the filling ratio w/Λ . Typical Starshot parameters [8] are assumed: payload mass 0.1 g, lightsail area 10 m^2 , and laser intensity 10 GW/m^2 .

tive indices of the constituent materials that dictate scattering properties, and payload mass that governs the degree of tradeoff between reflectivity and lightsail mass. To address those possibilities, we explore two types of dielectric materials of distinct refractive indices, as well as various values of payload mass. Without further specification, we assume typical Starshot parameters in which a laterally uniform, linearly polarized laser beam of intensity 10 GW/m^2 and wavelength $\lambda_0 = 1.2 \text{ }\mu\text{m}$ is incident normally on a lightsail of area 10 m^2 . To allow large design space, we consider fine grid size $\lesssim 10 \text{ nm}$, leading to at least 10^4 spatial design variables per $1 \text{ }\mu\text{m}^2$ in each layer. We consider two choices of material on each grid point: the target material and a vacant space with unity refractive index and negligible mass, which in practice can be vacuum or aerogels [44]. In case of vacuum, a low-index substrate is needed for mechanical rigidity, which can be treated as payload mass.

We begin by studying the optimizations of a representative high-index material, crystalline silicon. To gain insights into optimization results, we start by treating the overall thickness as a hyperparameter, namely, optimizing over period and material distributions at each thickness independently. The FOM (red solid line) and material volume filling ratio (black dashed line) of the optimal structures are summarized in Fig. 2(a), uncovering three distinct regimes of structural choices. First, at small thickness $\lesssim 20 \text{ nm}$, as may be expected, the optimization converges to a finite-thickness uniform slab (green region) since at deep subwavelength thicknesses, the reflectivity of high-index material increases more steeply than mass with filling ratio.

Second, for the intermediate thickness range we obtain the globally optimal solution. Surprisingly, even though we are optimizing over multiple independent layers of $N \gtrsim 2$ and material distributions on 2D grids, the optimal shape is a 1D grating (orange region), depicted in the upper Fig. 2b. With increasing thickness that allows for enhanced scattering, the optimal filling ratio, w/Λ , decreases in favor of lighter

mass, with simultaneously enhanced average reflectivity in the Doppler-shift bandwidth, resulting in dramatically decreasing D that exhibits a minimum at thickness 107 nm (denoted as Grating *A* in Fig. 2(a)). Furthermore, we observe that while the optimal period Λ also varies with thickness, it is always subwavelength $< \lambda_0$, e.g. $\Lambda = 1.08 \text{ }\mu\text{m}$ for Grating *A*. Such a subwavelength grating eliminates the diffraction in normal directions, which is important for enhancing the optical force along the normal direction. Compared to previously explored structures [8], the acceleration distance of Grating *A* is $D_{\text{Si}} \approx 1.9 \times 10^9 \text{ m}$, which represents a nearly 50% improvement.

In another context, 1D gratings have been proposed as broadband reflectors, known as high-contrast subwavelength gratings [32]. They have been demonstrated to achieve nearly 100% reflection over a bandwidth $\Delta\lambda/\lambda \gtrsim 30\%$ for either TE or TM polarized light, arising from the destructive interference of two guided modes that prohibits transmission. We examine if similar mechanism is the source of the performance of our optimized Grating *A* by plotting its reflection spectrum in Fig. 2(c). A Fano resonance feature is visible near the Doppler shift range, demonstrating that the high broadband reflectivity is indeed attributed to the double-mode interference effects. Another important observation is that for the incident light polarized along the *x*-axis, denoted in Fig. 2(b), the algorithm always finds a grating extending along the same *x*-direction. This is consistent with previous studies [33] that gratings parallel to the light polarization direction, when compared to those of perpendicular orientations, can achieve broadband reflection with smaller filling ratio, and consequently lighter mass. To gain more insights into the optimization process, in Fig. 2(d), we show the reflectivity plot of Grating *A* as a function of wavelength and filling ratio for a fixed thickness and period. Indeed, high reflection mostly occurs in the non-diffractive region, $\lambda > \Lambda$. As the filling ratio decreases, the bandwidth of the high reflection region shrinks, a typical tradeoff between the mass and average reflectivity.

To minimize D , the algorithm compromises on a minimal filling ratio (red dashed line) that does not degrade the reflectivity significantly. The $h(\beta)$ -weighted average reflection at the optimal filling ratio is around 75%.

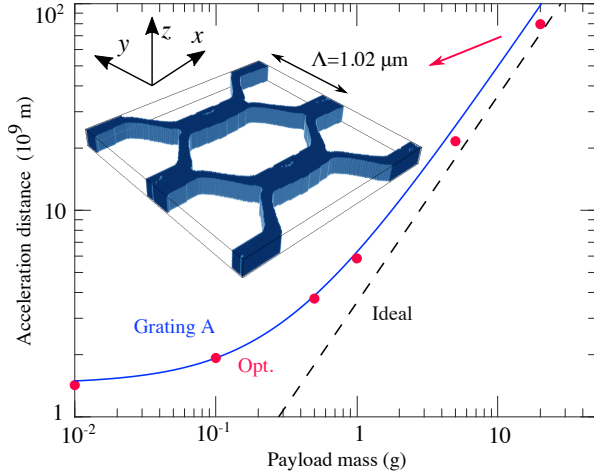


Figure 3: The acceleration distance as a function of payload mass for optimized structures (red dots), Grating A of Fig. 2 optimized for a payload mass 0.1 g (blue solid line), and ideal massless perfect reflector (black dashed line). (Inset): the optimal structure for payload mass 20 g.

Third, at even larger thickness, the emphasis shifts to minimizing the volume filling ratio for mass reduction, as there is little room for further improvement of reflectivity that is bounded by 100%. Two strategies are observed in our optimization results: when multiple layers $N \gtrsim 2$ are to be optimized, the optimal shape is a 1D grating with reduced thickness obtained by setting several layers to be vacant; alternatively, when the material is ensured to fill up the overall thickness by setting $N = 1$, the optimal structure switches to more complicated 2D PhC structures (blue region). For example, the optimal geometry at thickness 500 nm and $N = 1$, denoted as B and depicted in the lower Fig. 2(b), is a hexagonal lattice that resembles a trimmed 1D grating, a clear indication of the tendency of mass reduction. Its reflection spectrum, as shown in Fig. 2(c), reveals the presence of multiple resonance peaks within the Doppler-shift bandwidth, contributing to the larger average reflection than that of Grating A. However, its FOM is still outperformed by Grating A.

Next we aim to generalize the above design criteria to other values of payload mass. At each value of payload mass, we simultaneously optimize over material distributions, period, and thickness. The FOMs of the optimal structures (red dots), Grating A (blue solid curve), and the ideal massless perfect reflector (black dashed line) are compared in Fig. 3. Over a wide range of payload mass, the FOM of Grating A turns out to be very close to the optimal design, demonstrating that the simple 1D grating is a robust optimal solution. For a large payload mass, the mass of the sail becomes less significant and the FOM depends almost entirely on the reflectivity, thus favoring structures of near-perfect reflection. For instance, for

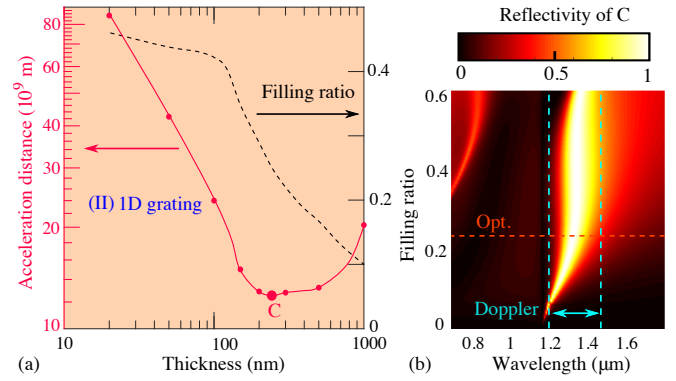


Figure 4: Inverse design of lightsail made of silicon nitride. (a) acceleration distance (left axis) and filling ratio (right axis) of structures optimized at each thickness, illustrate that over the entire range, the optimal geometry is a one-dimensional grating (orange). (b) the reflectivity of the optimal grating structure C as a function of filling ratio (w/Λ) and wavelength.

a payload mass of 20 g, the optimal structure is a honeycomb lattice (inset), whose average reflectivity approaches 95%.

Finally, we apply these optimization techniques to a lower-index constituent material, silicon nitride for its appealing mechanical properties [9]. Different structural choice is expected as lower-index medium reflects light more weakly. As shown in Fig. 4 (a), the optimal structure is exclusively a 1D grating (orange region) throughout the entire range of thickness [10, 1000] nm. The reason for ruling out the two other shapes as optimal solutions is as follows: at deep subwavelength thicknesses, reflection increases less dramatically than mass with filling ratio so that the uniform slabs that obtained for the high index material are not viable optimized solution here; at larger thicknesses, there is still much room for improvement of reflectivity, eliminating the need of cutting down on mass with 2D structuring. The globally optimal solution, denoted as Grating C , occurs at a larger thickness 243 nm with a subwavelength period $\Lambda = 1.17 \mu\text{m}$. Its reflectivity plot as a function of wavelength and filling ratio is shown in Fig. 4 (b), exhibiting narrower high-reflectivity band than the silicon medium. Therefore, similar compromise is made to decide on a minimal filling ratio, resulting in a moderate average reflection 57% and larger acceleration distance $D_{\text{SiN}} \approx 13 \times 10^9$ m. The degraded FOM might also be attributed to the large mass density of silicon nitride, which is around 35% higher than that of silicon. We examine this possibility by optimizing over a fictitious silicon nitride with the same mass density of silicon. The optimal structure is found to be almost identical to that of the real silicon nitride, which leads to slightly improved $D \approx D_{\text{SiN}}/1.35$, suggesting that the refractive index plays a more significant role.

Concluding remarks. We have developed an optimization framework that can effectively uncover optimal structure criteria for efficient lightsail propulsion. Under typical Starshot parameters, the lightsail geometry obtained by employing our optimization is a 1D subwavelength grating that outperforms

the FOM of previous optimal structures by almost 50%. To ensure that we approach the globally optimal solutions, we expect future work on deriving a tight theoretical bound with methods such as Lagrange duality and energy conservation relations [21]. We envision that our optimization framework can be further applied to other challenges in the lightsail project, including thermal management [12] and propulsion stability [14, 15].

Acknowledgements. We would like to thank Dr. Zin Lin, Dr. Ian Williamson, Dr. Momchil Minkov, Dr. Viktor Asadchy, Dr. Bo Zhao, and Cheng Guo for useful discussions. This work is supported by the Breakthrough Starshot Initiative, and used the Extreme Science and Engineering Discovery Environment (XSEDE) supported by the National Science Foundation, at the San Diego Supercomputing Center through allocation TG-MCA03S007.

-
- [1] L. Novotny and B. Hecht, *Principles of nano-optics* (Cambridge university press, 2012).
- [2] J. R. Moffitt, Y. R. Chemla, S. B. Smith, and C. Bustamante, *Annu. Rev. Biochem.* **77**, 205 (2008).
- [3] D. Gao, W. Ding, M. Nieto-Vesperinas, X. Ding, M. Rahman, T. Zhang, C. Lim, and C.-W. Qiu, *Light: Science & Applications* **6**, e17039 (2017).
- [4] J. Mansell, D. A. Spencer, B. Plante, A. Diaz, M. Fernandez, J. Bellardo, B. Betts, and B. Nye, in *AIAA Scitech 2020 Forum* (2020), p. 2177.
- [5] P. Lubin, arXiv preprint arXiv:1604.01356 (2016).
- [6] K. L. Parkin, *Acta Astronautica* **152**, 370 (2018).
- [7] N. Kulkarni, P. Lubin, and Q. Zhang, *The Astronomical Journal* **155**, 155 (2018).
- [8] H. A. Atwater, A. R. Davoyan, O. Ilic, D. Jariwala, M. C. Sherrott, C. M. Went, W. S. Whitney, and J. Wong, *Nature Materials* **17**, 861 (2018).
- [9] J. P. Moura, R. A. Norte, J. Guo, C. Schäfermeier, and S. Gröblacher, *Optics Express* **26**, 1895 (2018).
- [10] M. Lingam and A. Loeb, arXiv preprint arXiv:2002.03247 (2020).
- [11] J. Bird, L. Petzold, P. Lubin, and D. Deacon, arXiv preprint arXiv:2002.04051 (2020).
- [12] O. Ilic, C. M. Went, and H. A. Atwater, *Nano Letters* **18**, 5583 (2018).
- [13] M. Noyes and M. Hart, *Proc. AO4ELT6* (2019).
- [14] O. Ilic and H. A. Atwater, *Nature Photonics* **13**, 289 (2019).
- [15] J. Siegel, A. Y. Wang, S. G. Menabde, M. A. Kats, M. S. Jang, and V. W. Brar, *ACS Photonics* **6**, 2032 (2019).
- [16] Z. Manchester and A. Loeb, *The Astrophysical Journal Letters* **837**, L20 (2017).
- [17] K. V. Myilswamy, A. Krishnan, and M. L. Povinelli, *Optics Express* **28**, 8223 (2020).
- [18] S. Molesky, Z. Lin, A. Y. Piggott, W. Jin, J. Vucković, and A. W. Rodriguez, *Nature Photonics* **12**, 659 (2018).
- [19] K. Yao, R. Unni, and Y. Zheng, *Nanophotonics* **8**, 339 (2019).
- [20] G. Angeris, J. Vuckovic, and S. P. Boyd, *ACS Photonics* **6**, 1232 (2019).
- [21] S. Molesky, P. Chao, and A. W. Rodriguez, arXiv preprint arXiv:2001.11531 (2020).
- [22] Y. E. Lee, O. D. Miller, M. H. Reid, S. G. Johnson, and N. X. Fang, *Optics Express* **25**, 6757 (2017).
- [23] P. S. Venkataram, S. Molesky, W. Jin, and A. W. Rodriguez, *Physical Review Letters* **124**, 013904 (2020).
- [24] W. Jin, S. Molesky, Z. Lin, and A. W. Rodriguez, *Physical Review B* **99**, 041403 (2019).
- [25] S. Molesky, W. Jin, P. S. Venkataram, and A. W. Rodriguez, *Physical Review Letters* **123**, 257401 (2019).
- [26] M. Minkov, I. A. Williamson, L. C. Andreani, D. Gerace, B. Lou, A. Y. Song, T. W. Hughes, and S. Fan, arXiv preprint arXiv:2003.00379 (2020).
- [27] L. A. Coldren, *Optical Engineering* **36**, 616 (1997).
- [28] B. Slovick, Z. G. Yu, M. Berding, and S. Krishnamurthy, *Physical Review B* **88**, 165116 (2013).
- [29] P. Moitra, B. A. Slovick, Z. Gang Yu, S. Krishnamurthy, and J. Valentine, *Applied Physics Letters* **104**, 171102 (2014).
- [30] P. Moitra, B. A. Slovick, W. Li, I. I. Kravchenko, D. P. Briggs, S. Krishnamurthy, and J. Valentine, *Acs Photonics* **2**, 692 (2015).
- [31] E. S. Harper, E. J. Coyle, J. P. Vernon, and M. S. Mills, *Physical Review B* **101**, 195104 (2020).
- [32] C. F. Mateus, M. C. Huang, Y. Deng, A. R. Neureuther, and C. J. Chang-Hasnain, *IEEE Photonics Technology Letters* **16**, 518 (2004).
- [33] V. Karagodsky, F. G. Sedgwick, and C. J. Chang-Hasnain, *Optics express* **18**, 16973 (2010).
- [34] Y. H. Ko and R. Magnusson, *Optica* **5**, 289 (2018).
- [35] J. Chen, J. Ng, Z. Lin, and C. Chan, *Nature Photonics* **5**, 531 (2011).
- [36] L. Dal Negro, *Optics of aperiodic structures: fundamentals and device applications* (CRC Press, 2013).
- [37] K. Svanberg, *SIAM journal on optimization* **12**, 555 (2002).
- [38] J. S. Jensen and O. Sigmund, *Laser & Photonics Reviews* **5**, 308 (2011).
- [39] X. Liang and S. G. Johnson, *Optics Express* **21**, 30812 (2013).
- [40] C. W. Hsu, B. Zhen, A. D. Stone, J. D. Joannopoulos, and M. Soljačić, *Nature Reviews Materials* **1**, 1 (2016).
- [41] W. Jin, *grcwa: rigorous coupled wave analysis supporting automatic differentiation with autograd*, <https://github.com/weiliangjinca/grcwa>.
- [42] V. Liu and S. Fan, *Computer Physics Communications* **183**, 2233 (2012).
- [43] D. D. Maclaurin and M. Johnson, *Autograd: Efficiently computes derivatives of numpy code* (2015).
- [44] M.-H. Jo, J.-K. Hong, H.-H. Park, J.-J. Kim, S.-H. Hyun, and S.-Y. Choi, *Thin Solid Films* **308**, 490 (1997).